Backflow-mediated domain switching in nematic liquid crystals

Janez Turk and Daniel Svenšek
Department of Physics, Faculty of Mathematics and Physics, University of Ljubljana, Jadranska 19, SI-1000 Ljubljana, Slovenia
(Received 21 December 2013; published 28 March 2014)

We study the dynamics of the nematic liquid crystal kickback effect upon removal of a primary electric field and its amplification by a perpendicular secondary electric field resulting in the formation of domains with a reverse director orientation. Using computational fluid dynamics, we show that the domain formation is a robust phenomenon that takes place also in the complex case of multiple irregular random Freedericksz domains in three dimension as they appear in a realistic experimental situation. We propose domain switching by kickback amplification as a tool for self-insertion of shell-like inhomogeneities into an otherwise perfectly uniform director field configuration.

DOI: 10.1103/PhysRevE.89.032508 PACS number(s): 61.30.Gd, 47.57.Lj, 47.65.−d

I. INTRODUCTION

A. Background

Problems involving hydrodynamic motion of the nematic liquid crystal as a result of director reorientation ("backflow") have been modeled mainly in terms of the Ericksen-Leslie continuum theory of the nematic liquid crystal [1–3]. In retrospective, for one-dimensional (1D) geometry, Clark and Leslie [4] gave a thorough approximative analysis of nematic relaxation upon removal of the electric or magnetic field; a complete numerical treatment of the problem was contributed by van Doorn [5]. 1D backflow dynamics in the twist cell was studied by Berreman [6,7]. Pieranski, Brochard and Guyon [8,9] studied, both theoretically and experimentally, one-dimensional dynamic behavior in a magnetic field for three geometries (twisted, planar to homeotropic, and homeotropic to planar), limited to near-critical fields. They gave the distortion wave vector and effective viscosity dependence on the magnetic-field strength. The instability against periodic distortion in the case of the Freedericksz transition (first observed by Carr [10]) was studied by Guyon *et al.* [11] for the 2D case, and by Hurd *et al.* [12] for three dimensions. The pattern formation in a rotating magnetic field was observed experimentally and accounted for by a numerical study based on the Ericksen-Leslie equations [13,14]. The increasing interest in the hydrodynamic description of pattern formation in fluids enriched also the studies of nematic and nematic polymer fluids in this aspect [15–20].

The interest in backflow effects reached its climax in the past decade, when the asymmetry of the nematic point defect annihilation process was observed experimentally [21]. The annihilation of the disclination pair was studied numerically in two dimensions. It was shown by two groups independently and with complementary numerical methods that the speed of the $1/2$ disclination is indeed larger than that of the $-1/2$ disclination due to the backflow [22–24]. This was then cleanly demonstrated by a joint experimental and theoretical study in a quasi-2D geometry [25]. The pair-annihilation asymmetry of various types of nematic defects was addressed subsequently [26–28].

The competing numerical methods used to approach the hydrodynamic part of the problems have been mainly the discretization of the generalized continuum Navier-Stokes equation [13,14,23–25,29–31] and the lattice-Boltzmann method (LBM) [22,32–36]. Alternative methods include smoothed particle hydrodynamics, radial basis function collocation methods, and other hybrid or semianalytic approaches [26,37–40].

B. The kickback effect

It is known that when switching off the external electric or magnetic field in a liquid-crystal (LC) cell or pixel, the transmission intensity bounces momentarily due to a backflow-generated *kickback* effect [5,6,30,31]. During this transient process, the central part of the external-field-aligned director field initially undergoes a reverse rotation caused by the hydrodynamic flow, which itself is generated by the gradients of the director rotation, Fig. 1. By reverse, we mean that the sense of the director rotation is opposite to the one that would occur due to the elastic forces, without the action of the flow.

A direct optical quantification of the kickback effect in the twist cell was presented in Ref. [41]. In practical LC cell operation, the kickback is undesirable and possibly minimized [42,43]. Its use for estimating the nematic viscosity coefficients is reported in Ref. [44].

C. Kickback amplification

In the present work, we exploit the kickback effect to generate spatial director structures dynamically. We demonstrate numerically that by applying a secondary perpendicular electric field (i.e., horizontal in Fig. 1) at moment when the primary electric field of comparable strength is removed, the originally weak kickback can be amplified to create a reverse domain. Moreover, we show that although the backflow generation depends on the director field boundary condition (anchoring direction with respect to the boundary normal), the kickback amplification is not at all restricted to a regular monodomain case such as the one presented in Fig. 1, but rather surprisingly turns out to be a robust phenomenon that takes place in each individual Freedericksz domain of an irregular multidomain sample. Furthermore, adopting the geometry of a LC cell and performing a full 3D numerical calculation, we confirm that the kickback amplification effect persists also in actual realistic circumstances and could thus be observed experimentally.

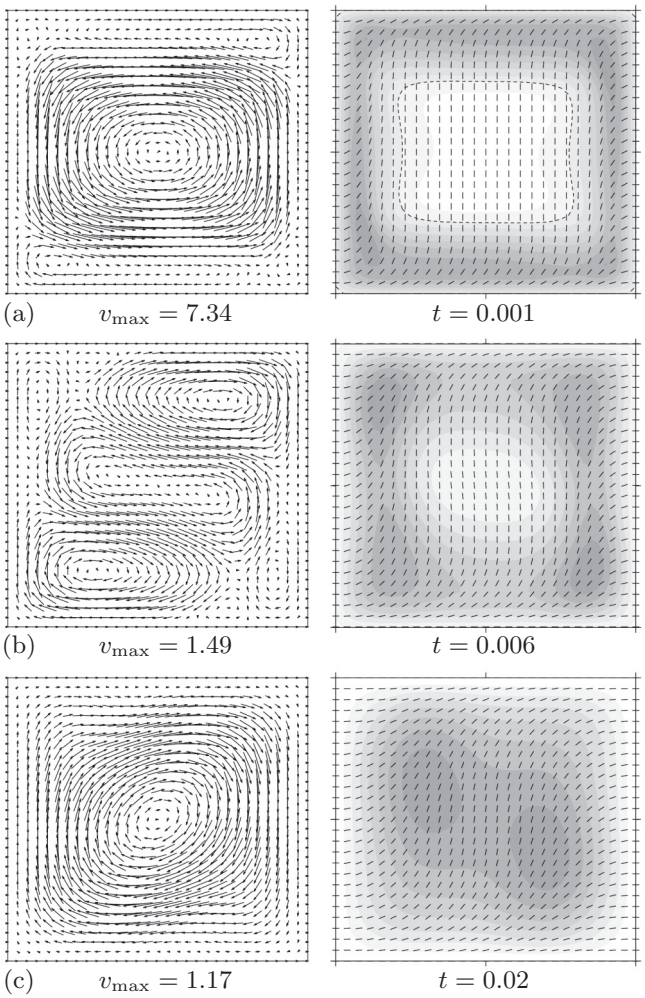

FIG. 1. Kickback in a 2D square cell (in-plane switching) upon removal of the in-plane vertical electric field [30]: subsequent snapshots [(a)–(c)] of the velocity fields (left column), director fields, and director angular velocity fields (schematically represented by levels of gray: darker levels represent faster clockwise rotation). Rigid anchoring in the horizontal direction is assumed at all four edges. The strength of the initial electric field is $E = 10$. The units are defined in Sec. II C. In the kickback phase (a) the director in the central region rotates reversely (counterclockwise in this example) due to the strong reverse backflow, which is generated predominantly by the horizontal boundaries. The region of the reverse rotation is depicted brightest and is encircled by the dashed contour line of the stationary director field. Note the weak reverse director deformation in the center (b), when the kickback transient has almost ceased and the backflow and the director rotation in the center are about to change direction (c).

II. THEORY AND METHOD

In our case, the nematodynamic variables are the unit nematic director $\mathbf{n}(\mathbf{r})$, $\mathbf{n}^2 = 1$, and the velocity field $\mathbf{v}(\mathbf{r})$. As usual, incompressibility is assumed for the latter. Both fields are dynamically coupled. The electric field is considered homogeneous. In the following, we recapitulate the rather extensive but closed system of nematodynamic equations [30,31,45,46] that has to be solved numerically.

The orientational elastic and dielectric free-energy density reads

$$f = \tfrac{1}{2}K_{11}(\nabla\cdot\mathbf{n})^2 \quad (1)$$

$$+ \tfrac{1}{2}K_{22}[\mathbf{n}\cdot(\nabla\times\mathbf{n})]^2 \quad (2)$$

$$+ \tfrac{1}{2}K_{33}[\mathbf{n}\times(\nabla\times\mathbf{n})]^2 \quad (3)$$

$$- \tfrac{1}{2}\varepsilon_a\varepsilon_0(\mathbf{E}\cdot\mathbf{n})^2, \quad (4)$$

where K_{11}, K_{22}, and K_{33} are the splay, twist, and bend elastic constants, respectively, $\mathbf{E}$ is the electric field, and ε_a is the dielectric anisotropy, assuming $\varepsilon_a > 0$. In one elastic constant (K) approximation, the bulk elastic free-energy density, Eqs. (1)–(3), reduces to

$$f = \tfrac{1}{2}K(\nabla\mathbf{n})^2. \quad (5)$$

Flexoelectricity is omitted from Eqs. (1)–(4). It can be shown that for typical values [47,48] of the thermotropic nematic flexoelectric coefficients $\sim 10^{-11}$ As/m, in the strongly deformed regions of the sample—the domain walls—it is actually comparable in magnitude with the dielectricity. Elsewhere, however, it is completely negligible. For strong electric fields used in this study, the domain walls represent only a small fraction of the system. Moreover, the relevant electric coupling takes place in the quasihomogeneous regions between the domain walls where the director is reoriented by the electric field, but not in the domain walls where it is left unchanged. One can therefore expect that the inclusion of flexoelectricity would affect the width of the domain walls and slightly modify the director gradients of nearby regions, which might result in small rescaling of the electric fields required for switching. Apart from this minor correction, the flexoelectricity can be safely discarded.

We define the "molecular field"

$$h_i = -\frac{\partial f}{\partial n_i} + \partial_j\left(\frac{\partial f}{\partial(\partial_j n_i)}\right). \quad (6)$$

The governing equations are then

$$\frac{\partial\mathbf{n}}{\partial t} = \left[\frac{1}{\gamma_1}\mathbf{h} - \frac{\gamma_2}{\gamma_1}\mathsf{A}\cdot\mathbf{n} - \mathsf{W}\cdot\mathbf{n} - (\mathbf{v}\cdot\nabla)\mathbf{n}\right]_{\perp\mathbf{n}}, \quad (7)$$

$$\rho\left[\frac{\partial\mathbf{v}}{\partial t} + (\mathbf{v}\cdot\nabla)\mathbf{v}\right] = -\nabla p + \nabla\cdot(\sigma^v + \sigma^e), \quad (8)$$

$$\nabla\cdot\mathbf{v} = \mathbf{0}, \quad (9)$$

where

$$\sigma^e_{ij} = -\frac{\partial f}{\partial(\partial_i n_k)}\partial_j n_k \quad (10)$$

is the elastic stress tensor,

$$\sigma^v = \alpha_1\mathbf{n}\otimes\mathbf{n}(\mathbf{n}\cdot\mathsf{A}\cdot\mathbf{n}) + \alpha_2\mathbf{n}\otimes\mathbf{N} + \alpha_3\mathbf{N}\otimes\mathbf{n} + \alpha_4\mathsf{A} + \alpha_5\mathbf{n}\otimes(\mathsf{A}\cdot\mathbf{n}) + \alpha_6(\mathsf{A}\cdot\mathbf{n})\otimes\mathbf{n} \quad (11)$$

is the reaction-viscous stress tensor,

$$A_{ij} = \tfrac{1}{2}(\partial_i v_j + \partial_j v_i), \quad W_{ij} = \tfrac{1}{2}(\partial_i v_j - \partial_j v_i), \quad (12)$$

N is the director rotation with respect to the background fluid,

$$\mathbf{N} = \dot{\mathbf{n}} + \mathsf{W} \cdot \mathbf{n}, \quad \dot{\mathbf{n}} = \frac{d\mathbf{n}}{dt}, \tag{13}$$

ρ is the density, α_i are Leslie "viscosity" coefficients linked with the relation $\alpha_6 - \alpha_5 = \alpha_3 + \alpha_2 \equiv \gamma_2$, and $\gamma_1 = \alpha_3 - \alpha_2$ is the rotational viscosity; γ_2/γ_1 is known as the reaction parameter [49]. Equation (7) is projected normal to **n** due to $\mathbf{n}^2 = 1$.

In the case of backflow, the left-hand side of Eq. (8) is usually set to zero, assuming a low Reynolds number and a quasistationary flow field to an excellent approximation. We nevertheless keep both terms as the regime may change for very strong electric fields (as explained in Sec. II B).

A. Material parameters

Elastic constants and viscosities of the thermotropic LC representative MBBA are used throughout this study because they are relatively well known [45]. The dielectric anisotropy is, however, assumed positive.

Approximate ratios of the elastic constants [45] at 22 °C are $K_{22}/K_{11} = 0.42$ and $K_{33}/K_{11} = 1.4$, where $K_{11} = 5 \times 10^{-12}$ N. Such elastic anisotropy is characteristic of thermotropic LCs, i.e., bend is typically the most expensive while twist is the cheapest. In our numerical calculations, we used both these ratios as well as the one elastic constant approximation. However, all the results presented in this paper are calculated with a single elastic constant in order to separate the backflow effects from possible influences of the elastic anisotropy.

For the Leslie coefficients, we take the ratios [45]

$$\begin{aligned}
\alpha_1/\alpha_4 &= 0.08,\\
\alpha_2/\alpha_4 &= -0.93,\\
\alpha_3/\alpha_4 &= -0.014,\\
\alpha_5/\alpha_4 &= 0.56,\\
\alpha_6/\alpha_4 &= -0.41,
\end{aligned}$$

which can be considered generic for flow-aligning thermotropic nematics consisting of rod-like molecules; $\alpha_4 = 0.08$ Pa s.

B. Scales

The time scale of the director field, Eq. (7), is

$$\tau_n = \frac{\gamma_1 \xi_E^2}{K}, \tag{14}$$

where $\xi_E = \sqrt{K/\varepsilon_a \varepsilon_0}/E$ is the electric coherence length. The time scale of the velocity field, Eq. (8), is

$$\tau_v = \frac{\rho L^2}{\gamma_1}, \tag{15}$$

where L is a typical system size and the effective fluid viscosity $\sim\gamma_1$. The ratio of the two time scales defines the unsteadiness parameter of the velocity field (Strouhal number Sr for periodic flows),

$$\mathrm{Sr} = \tau_v/\tau_n = \frac{L^2}{\xi_E^2}\frac{\rho K}{\gamma_1^2} \sim \frac{L^2}{\xi_E^2} \times 10^{-6}. \tag{16}$$

The characteristic magnitude of the velocity is estimated by equating the magnitudes of representative active ($\gamma_1 \dot{\mathbf{n}}$) and passive ($\alpha_4 \mathsf{A}$) terms of the viscous stress tensor, Eq. (11),

$$v_0 = \frac{KL}{\gamma_1 \xi_E^2}. \tag{17}$$

The Reynolds number $\mathrm{Re} = \rho v_0 L/\gamma_1$ is then

$$\mathrm{Re} = \frac{L^2}{\xi_E^2}\frac{\rho K}{\gamma_1^2} \sim \frac{L^2}{\xi_E^2} \times 10^{-6}. \tag{18}$$

In backflow dynamics, we are thus normally in the regime of very low Re and Sr. At high electric fields (small ξ_E), however, both dimensionless numbers will increase and may come closer to unity. For $L/\xi_E = 200$, which we will use in some examples, $\mathrm{Re} = \mathrm{Sr} \sim 0.04$. This is particularly important for short but critical transients, and the kickback is a good example of just such delicacy.

C. Units

Lengths are measured relative to the shortest geometrical dimension of the system, which we denote L. In the 2D examples, it is the side of the square, whereas in the 3D case it is the thickness of the LC cell. The corresponding time unit is

$$\tau = \frac{\gamma_1 L^2}{K}. \tag{19}$$

The unit for the electric field is

$$E_0 = \frac{1}{L}\sqrt{\frac{K}{\varepsilon_a \varepsilon_0}}, \tag{20}$$

which is the electric field strength with the coherence length that equals L.

D. Method of solution

The system of nematodynamic equations (7)–(9) is solved by an open-source finite volume solver [51] for transient flows, which was substantially adapted and augmented for the specific nematodynamic situation. The advection term of Eq. (8) is included. A homogeneous rectilinear mesh was used, sufficiently fine to describe the domain walls. The mesh size is given with each example.

III. 2D MONODOMAIN SWITCHING

We use this minimal but clean example, Fig. 2, to demonstrate the basic mechanism of domain creation by kickback amplification that was pointed out in Sec. I C. In one elastic constant approximation, the critical field of the Freedericksz transition in the square geometry is $E_c = \sqrt{2}\pi \approx 4.44$. Assuming rigid anchoring, the middle part of the sample is aligned by the in-plane vertical electric field $E_1 = 35$. At the moment when this primary field is turned off, an in-plane horizontal electric field $E_2 = 35$ is applied, which amplifies the backflow-generated kickback distortion and results in a domain of reverse director orientation.

The reverse domain is then shrinking by a curvature-driven process [50], where the speed of a part of the domain wall is proportional to the local curvature. The radius R of a circular

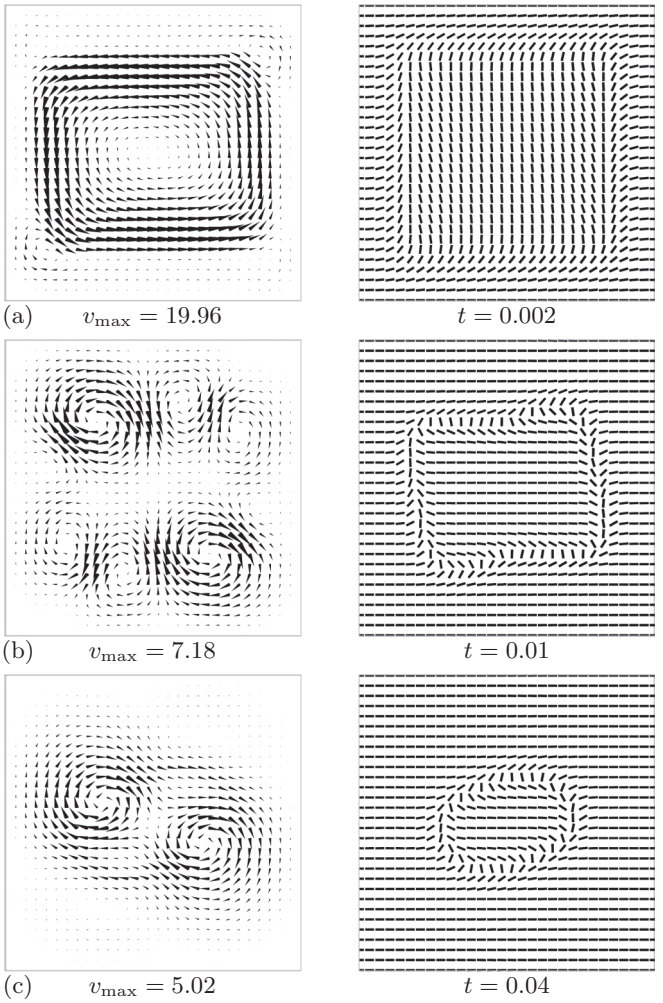

FIG. 2. Kickback in a 2D square cell, amplified by a horizontal field, leading to the formation of a reverse domain followed by its slow shrinking. Subsequent snapshots [(a)–(c)] of the velocity (left column) and director fields are shown. The velocity scales are larger than in Fig. 1 due to the presence of the electric field. $E_1 = E_2 = 35$.

domain is thus decreasing with a rate $\propto 1/R$. For a general shape, it follows by integration that the area of the domain decreases at a rate that is constant in time [50]. The formation of the reverse domain is a fast process, accomplished in time τ_n, whereas its shrinking gets slow with increasing domain size. The domain is thus typically long-lived in comparison with other time scales of the system.

A numerical diagram for the required primary and secondary field strengths E_1 and E_2 required for switching in the 2D square geometry of Fig. 2 is presented in Fig. 3. In units of E_0, the fields are empirically related by

$$\frac{1}{E_1^2} + \frac{1}{E_2^2} \lessapprox \frac{1}{(5E_c)^2}, \tag{21}$$

or in other words

$$\xi_{E_1}^2 + \xi_{E_2}^2 \lessapprox \frac{1}{500} \tag{22}$$

(a circle), where ξ_{E_1} and ξ_{E_2} are the corresponding electric coherence lengths (in units of L).

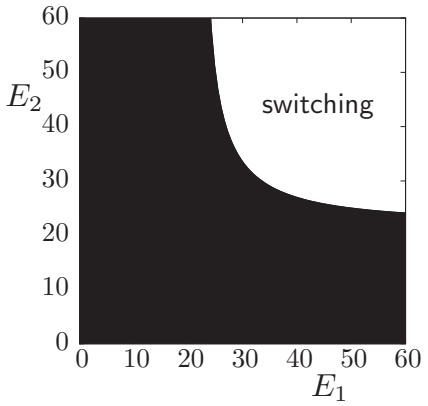

FIG. 3. Primary and secondary field strengths, E_1 and E_2, required for switching.

There exist several issues regarding the extrapolation of this 2D monodomain switching to more general and realistic circumstances. In the presented example, the role of the anchoring at the boundaries is crucial for the generation of the backflow as a response to the director reorientation. In a larger sample, the domains of the Freedericksz transition are scattered all over the system and are of irregular shapes. In particular, if one applies strong electric fields in order to get a good amplification of the kickback and well-defined reverse domains, the original Freedericksz domains are numerous. Thus, the situation is quite different from the monodomain example of Fig. 2—there are no boundaries with anchoring that would encircle the domains, and hence the generation of the backflow is in question. The situation gets still more complex in 3D geometry, which is not just a straightforward extension of the 2D case.

IV. 2D MULTIDOMAIN SWITCHING

Increasing the system size or, equivalently, increasing the electric field strength, increases the number of Freedericksz domains. Starting with a tiny random perturbation of a uniform director field and applying a strong primary electric field, one gets a large number of small random domains with size $\sim\xi_E$, Fig. 5 at $t = 0.0001$ (see Fig. 4 for an illustration of the color and grayscale legend for the selected director component). For a well-pronounced kickback, however, one requires domains with diameters large compared to the width of the domain walls, Fig. 2, so that the interior of the domain is well aligned with the electric field and thus the elastic forces are weak.

Therefore, one first applies the primary electric field and then waits for the small domains to coalesce, Fig. 5, before

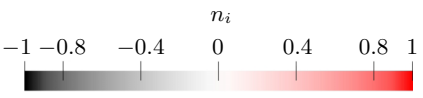

FIG. 4. (Color online) Color and grayscale legend for the selected director component applies to all subsequent figures. In grayscale, black domains are darker than red domains (cf. Fig. 6).

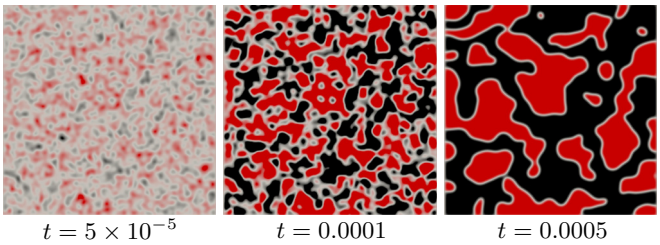

FIG. 5. (Color online) Coalescence of Freedericksz domains over the course of time. $E_1 = 200$, mesh size is 300×300. The color and grayscale coding, Fig. 4, represents the vertical component n_y of the director.

switching the fields. To be switched, a domain must reach at least a switchable size ξ_s. It can be estimated on the basis of Eq. (21) as follows. Equation (21) gives the electric-field strengths required to switch the system of size L, which can also be interpreted as switching a domain of this size. The nematodynamic system, Eqs. (7)–(9), is invariant with respect to rescaling the length, provided that time and the electric field are rescaled according to Eqs. (19) and (20). Hence, downscaling the domain size from L to ξ_s, Eq. (21) remains valid if E_1 and E_2 are rescaled accordingly:

$$\frac{1}{E_1^2} + \frac{1}{E_2^2} \lessapprox \left(\frac{\xi_s}{5E_c}\right)^2, \tag{23}$$

which thus serves as the estimate of the domain switchable size ξ_s for given E_1 and E_2.

The numeric results show, rather surprisingly, that the switching of the coalesced configuration of several irregular domains works perfectly, Fig. 6. The kickback mechanism described for the regular case of Sec. III thus applies also to the general case of multiple domains. Instead of the anchoring at the cell boundaries as in Fig. 2, in this case the director in domain walls is immobilized by the secondary electric field and the neighboring domains. Hence, the kickback amplification takes place individually in each domain if only it is large enough, irrespective of the irregularity of domain shapes and positions.

Apart from the global $n_y \to n_x$ transformation, the switched state [Fig. 6(b)] is actually quite similar to the original configuration of Freedericksz domains [Fig. 6(a)], with one important distinction. The switched director field is aligned with the electric field everywhere except at the domain walls—it is thus perfectly homogeneous but with ringlike inclusions. Turning off the secondary electric field will alter the shrinking dynamics of the reverse domains but will not affect the global director configuration. The original Freedericksz configuration, in contrast, is frustrated by the anchoring and the primary electric field and would disintegrate from the boundary and from the domain walls if this field were removed. The domain switching by kickback amplification is thus a mechanism for self-insertion of ringlike deformation objects into an otherwise perfectly uniform director field configuration.

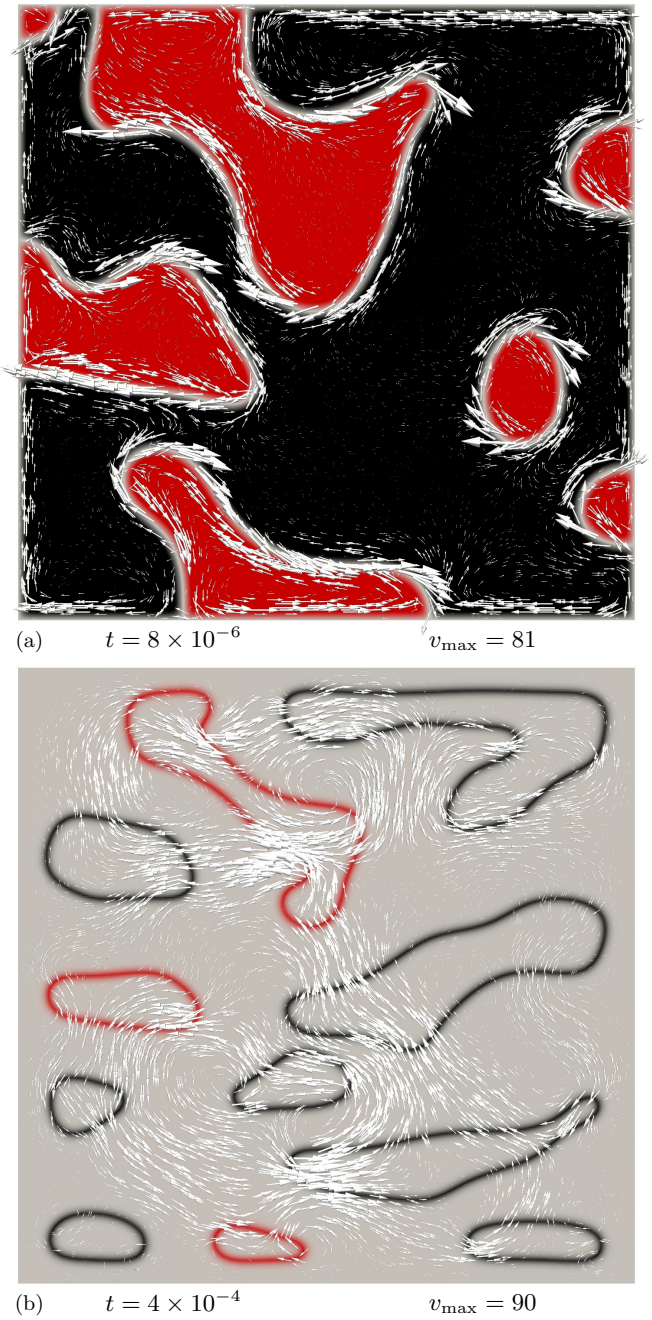

FIG. 6. (Color online) Multiple domain switching in two dimensions. $E_1 = E_2 = 200$, mesh size is 300×300, n_y is coded according to Fig. 4. Initially, shortly after the application of the secondary electric field, the backflow is concentrated at the domain walls (a). As a contrast, when the switched domains are slowly shrinking (b), the flow is global.

V. SWITCHING IN THREE DIMENSIONS

A. Monodomain in a cube

Let us first inspect the switching of a cubic Freedericksz monodomain—a situation analogous to the 2D monodomain case of Fig. 2. The anchoring is along x on all faces of the cell, while the primary and secondary electric fields point along z and x, respectively. The monodomain configuration exhibits

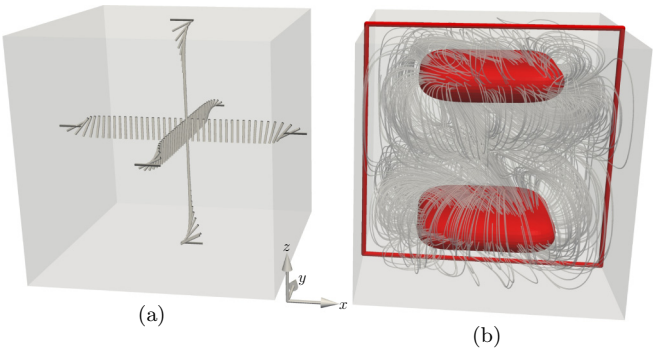

FIG. 7. (Color online) A cubic monodomain in an electric field along z exhibits three types of domain walls at its boundaries (a). Reverse domains of the switched configuration (the secondary electric field is along x) are presented by the enclosing contour surfaces; the flow field is represented by the stream lines (b). $E_1 = E_2 = 70$, mesh size is $80 \times 80 \times 80$. A 2D cross section shown in Fig. 8 is indicated by the frame (b).

three types of domain walls at its boundaries, Fig. 7(a). As in the 2D monodomain case, the predominant generator of the backflow upon removal of the electric field is the horizontal boundary, whereas the twist deformation (xz faces) generates no flow at all. The flow-generating forces are thus similar to those in the 2D case, Fig. 2, with the square lying in the xz plane. Due to the extra dimension, however, the velocity field is now viscously screened by the velocity gradient in the y direction and is thus substantial only in the region where the body force is actually exerted on the fluid, Fig. 8(a), to be compared with the unscreened 2D flow in Fig. 2. As a result, the domain is not switched as a whole, but only in the neighborhood of the horizontal faces, Fig. 7(b). It turns out that for lower field strengths, the two reverse domains are not completely detached but remain connected by a narrower reverse region in the middle to form an anvil-like switched domain [such domains can be seen in Fig. 10(b)]. In Fig. 8, the switching sequence is demonstrated for the 2D cross section indicated in Fig. 7(b).

Shrinking the extra dimension, i.e., flattening the cube in the y direction in order to arrive at the geometry of a usual LC planar cell, makes the screening obviously even severer. Therefore, the in-plane domain switching in the planar cell would not work. The 2D examples in Figs. 2 and 6 are thus nicely illustrating the switching mechanism, but they cannot be directly extrapolated to the in-plane switching in the planar cell.

B. Random domains in a planar LC cell

Finally, we present the practical example—switching of many irregular random domains in the geometry of a usual planar LC cell. This example should be readily accessible to experiments. The thickness of the LC cell (z axis) is L (the length unit according to Sec. II C), whereas the lateral dimensions are $10L$ for demonstration purposes, which is already in the large limit. All directions are the same as in Sec. V A. Neglecting the insignificant lateral faces, the anchoring is thus planar with an easy axis in the x direction. The primary electric field E_1 is normal to the cell.

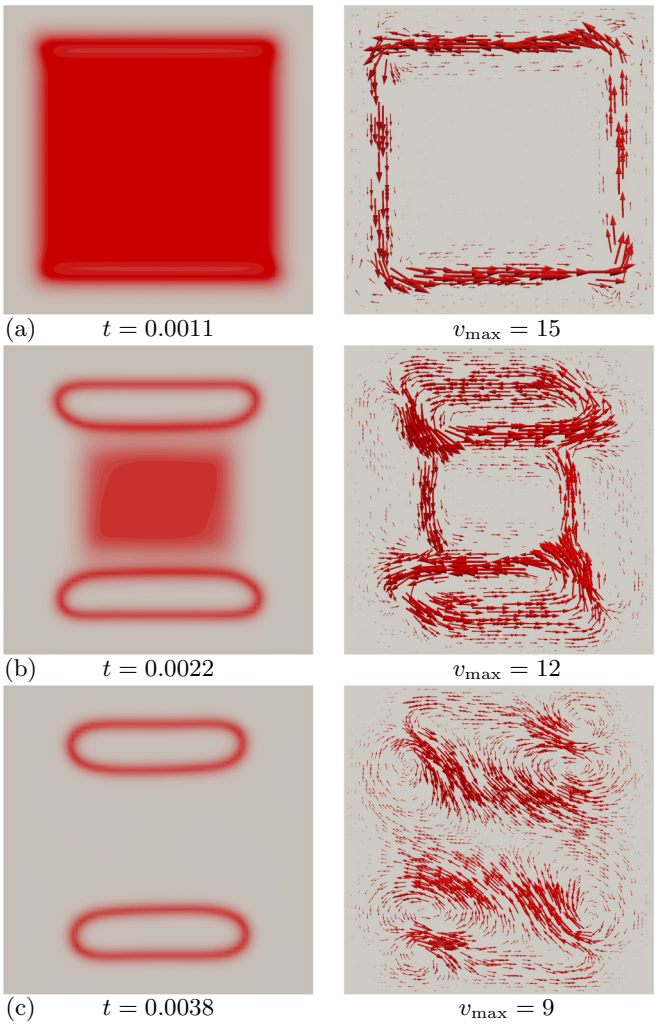

FIG. 8. (Color online) The xz cross section through the center of the cube indicated in Fig. 7(b): subsequent snapshots [(a)–(c)] of director fields (left) (with n_z coded according to Fig. 4) and velocity fields. Note the screened flow (a).

The secondary electric field E_2 is in-plane, parallel to the anchoring direction, and is thus in practice realized by in-plane electrodes.

The strength of both electric fields will be $E_1 = E_2 = 35$. The size of the Freedericksz domains before the switching should be at least L, so that there is only a single layer of domains sandwiched in the cell for the sake of simplicity (in principle, there is no such restriction, as we learned in Fig. 6). The formation of sufficiently large domains by coalescence is illustrated in Fig. 9. The configuration of domains ready for switching is shown in Fig. 10(a), whereas

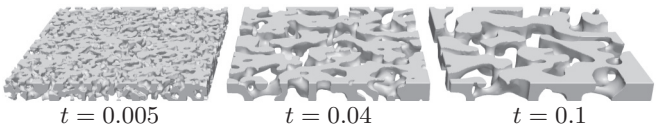

FIG. 9. Coalescence of Freedericksz domains created by a primary electric field $E_1 = 35$ normal to the cell plane.

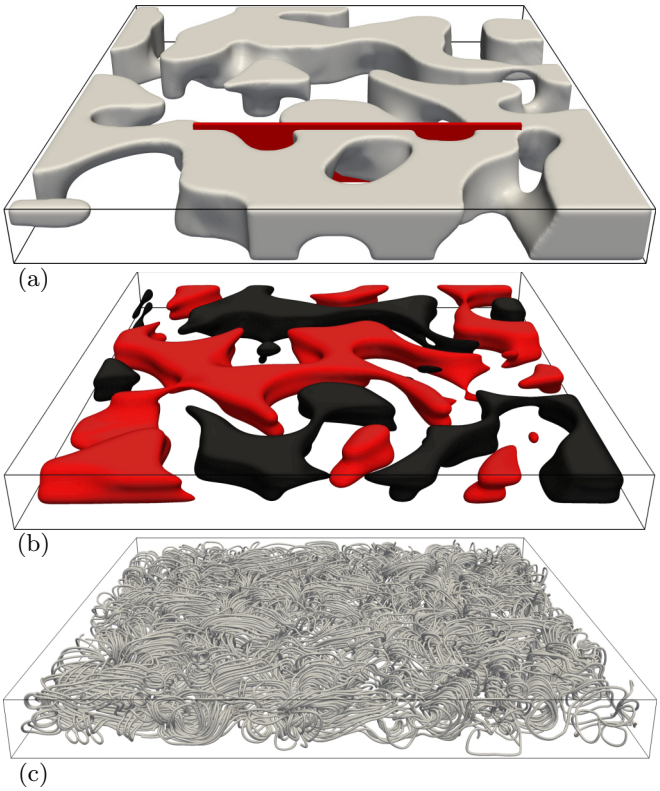

FIG. 10. (Color online) (a) Freedericksz domains just before the switching. The director points, e.g., up outside the contour surface and down inside it. The rectangle indicates the 2D cross section shown in Fig. 11. (b) Snapshot of the switched state. The reverse domains lie *inside* the contour surfaces; n_z is coded according to Fig. 4. Note their anvil-like vertical shape. Velocity streamlines (c) of the switched state in the same moment, showing the localization of the flow to individual domains. $E_1 = E_2 = 35$, mesh size: $300 \times 300 \times 30$.

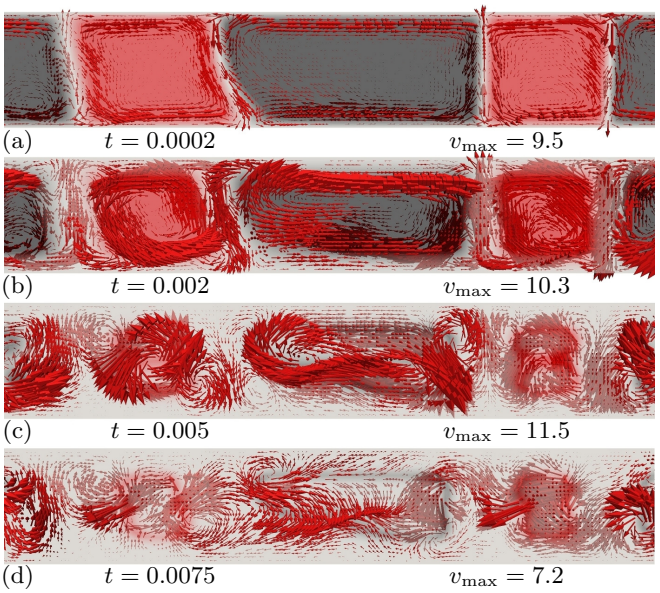

FIG. 11. (Color online) The xz cross section indicated by the rectangle in Fig. 10(a): subsequent snapshots [(a)–(d)] of superimposed director fields (with n_z coded according to Fig. 4) and velocity fields.

the switched configuration is depicted in Figs. 10(b) and 10(c). The omnipresent anvil-like vertical shape of the reverse domains is a sign of viscous screening of the backflow—compare Fig. 7(b). Unlike in that case, the velocity gradients responsible for the screening are not due to the no-slip cell boundaries but to adjacent domains in the y direction exhibiting opposite flow. In Fig. 11, the switching sequence is demonstrated for the rectangular cross section indicated in Fig. 10(a). In Fig. 11(a), we see the initial (screened) backflow generated by the decaying Freedericksz domains, which drives the director kickback in the interior of these domains. In Fig. 11(d), the switching is complete and the backflow is driven by the shrinking of reverse domains analogous to Fig. 8(c).

C. Connection with experimental scales

Let us also give an example of concrete length, time, and electric-field scales for the case of Sec. V B. Assuming a LC cell thickness of $L = 20$ μm, the characteristic domain switching time is $\tau_n \approx 5$ ms. The maximum flow velocities of Fig. 11 are ~ 35 μm/s. The width of the domain walls is ~ 0.2 μm, which should be compared with the anchoring extrapolation length to ensure rigid anchoring conditions. Assuming a dielectric anisotropy $\varepsilon \sim 10$, the corresponding strength of the primary and secondary electric fields is $E_1 = E_2 \sim 2$ V/μm.

VI. CONCLUSIONS

We have presented a backflow-mediated domain switching dynamics in nematic liquid crystals, starting with a simple system in a simple geometry to illustrate the essence of the mechanism, eventually arriving at the realistic 3D example that works in practice and should be accessible to experiments. It is one of the rare processes in liquid crystals in which the hydrodynamic flow generated by the director reorientation—the backflow—does not introduce just minor corrections but is of decisive importance. The presented domain switching mechanism relies critically on the backflow and could therefore be used to determine some of the dynamic material parameters of the nematic liquid crystal with great accuracy.

The domain switching by kickback amplification appears as a sophisticated dynamic mechanism for self-insertion of shell-like director inhomogeneities into a uniform director field configuration via the intermediate structural (Freedericksz) transition. The switched state is completely decoupled from this intermediate Freedericksz state, which is merely transient. After switching, the system undergoes a slow shrinking dynamics, driven solely by the curvature of the domain walls. Depending on the type of liquid crystal (low-molecular-mass thermotropic, lyotropic, polymeric), the shrinking can proceed in a wide span of time scales. The different dynamic stages could be potentially arrested and frozen in by a comparatively quick polymerization and gelation process, e.g., to be inspected offline one by one, or to yield a fixed structure with spatially modulated optical properties. The profiles can be controlled,

e.g., by tuning the waiting time before the switching, the strength of the electric field, the shrinking time before the gelation, etc.

Let us conclude with a speculation. If $\xi_{E_{1,2}}$ are much smaller than the thickness of the LC cell, would it be possible to generate a second kickback of the already switched domain by turning off the secondary electric field and restoring the primary electric field? Would it even be possible to generate a cascade of sequential switching processes? These would be interesting as they would yield a quasiperiodic dynamics, spontaneously localized to reorientation and flow cells. Such spontaneous dynamic patterning is one of the possible aspects one should address in a potential experiment.

ACKNOWLEDGMENTS

The authors acknowledge the support of the Agency for Research and Development of Slovenia (Grants No. J1-4297 and No. J1-4134).

[1] J. L. Ericksen, Arch. Ration. Mech. Anal. **4**, 231 (1960).
[2] F. M. Leslie, Q. J. Mech. Appl. Math. **19**, 357 (1966); Arch. Ration. Mech. Anal. **28**, 265 (1968).
[3] P. C. Martin, O. Parodi, and P. S. Pershan, Phys. Rev. A **6**, 2401 (1972).
[4] M. G. Clark and F. M. Leslie, Proc. R. Soc. London, Ser. A **361**, 463 (1978).
[5] C. Z. van Doorn, J. Physique **36**, C1-261 (1975).
[6] D. W. Berreman, J. Appl. Phys. **46**, 3746 (1975).
[7] D. W. Berreman, J. Appl. Phys. **50**, 8016 (1979).
[8] F. Brochard, P. Pieranski, and E. Guyon, Phys. Rev. Lett. **28**, 1681 (1972).
[9] P. Pieranski, F. Brochard, and E. Guyon, J. Phys. **34**, 35 (1973).
[10] E. F. Carr, Mol. Cryst. Liq. Cryst. **34**, 159 (1977).
[11] E. Guyon, R. Meyer, and J. Salan, Mol. Cryst. Liq. Cryst. **54**, 261 (1979).
[12] A. J. Hurd, S. Fraden, F. Lonberg, and R. B. Meyer, J. Phys. **46**, 905 (1985).
[13] K. B. Migler and R. B. Meyer, Phys. Rev. Lett. **66**, 1485 (1991).
[14] K. B. Migler and R. B. Meyer, Phys. Rev. E **48**, 1218 (1993).
[15] M. Kaiser, W. Pesch, and E. Bodenschatz, Physica D **59**, 320 (1992).
[16] H. R. Brand, C. Fradin, P. L. Finn, W. Pesch, and P. E. Cladis, Phys. Lett. A **235**, 508 (1997).
[17] E. Plaut, W. Decker, A. G. Rossberg, L. Kramer, W. Pesch, A. Belaidi, and R. Ribotta, Phys. Rev. Lett. **79**, 2367 (1997).
[18] A. D. Rey and T. Tsuji, Macromol. Theor. Simul. **7**, 623 (1998).
[19] E. Plaut and W. Pesch, Phys. Rev. E **59**, 1747 (1999).
[20] J. J. Feng, J. Tao, and L. G. Leal, J. Fluid Mech. **449**, 179 (2001).
[21] P. E. Cladis and H. R. Brand, Physica A **326**, 322 (2003).
[22] G. Tóth, C. Denniston, and J. M. Yeomans, Phys. Rev. Lett. **88**, 105504 (2002).
[23] D. Svenšek and S. Žumer, Phys. Rev. E **66**, 021712 (2002).
[24] D. Svenšek and S. Žumer, Phys. Rev. Lett **90**, 155501 (2003).
[25] C. Blanc, D. Svenšek, S. Žumer, and M. Nobili, Phys. Rev. Lett. **95**, 097802 (2005).
[26] A. M. Sonnet and E. G. Virga, Liq. Cryst. **37**, 785 (2010).
[27] I. Dierking, M. Ravnik, E. Lark, J. Healey, G. P. Alexander, and J. M. Yeomans, Phys. Rev. E **85**, 021703 (2012).
[28] P. Biscari and T. J. Sluckin, Eur. J. Appl. Math. **23**, 181 (2012).
[29] J. Bajc, G. Hillig, and A. Saupe, J. Chem. Phys. **106**, 7372 (1997).
[30] D. Svenšek and S. Žumer, Liq. Cryst. **28**, 1389 (2001).
[31] D. Svenšek and S. Žumer, Continuum Mech. Thermodyn. **14**, 231 (2002).
[32] C. Denniston, E. Orlandini, and J. M. Yeomans, Phys. Rev. E **63**, 056702 (2001).
[33] C. Denniston, G. Toth, and J. M. Yeomans, J. Stat. Phys. **107**, 187 (2002).
[34] C. M. Care, I. Halliday, K. Good, and S. V. Lishchuk, Phys. Rev. E **67**, 061703 (2003).
[35] T. J. Spencer and C. M. Care, Phys. Rev. E **74**, 061708 (2006).
[36] A. Sengupta, U. Tkalec, M. Ravnik, J. M. Yeomans, C. Bahr, and S. Herminghaus, Phys. Rev. Lett. **110**, 048303 (2013).
[37] A. M. Sonnet and E. G. Virga, Liq. Cryst. **36**, 1185 (2009).
[38] M. V. Yakutovich, C. M. Care, C. J. P. Newton, and D. J. Cleaver, Phys. Rev. E **82**, 041703 (2010).
[39] J. P. Hernandez-Ortiz, B. T. Gettelfinger, J. Moreno-Razo, and J. J. de Pablo, J. Chem. Phys. **134**, 134905 (2011).
[40] P. A. Cruz, M. F. Tome, I. W. Stewart, and S. McKee, J. Comput. Phys. **247**, 109 (2013).
[41] N. J. Smith, M. D. Tillin, and J. R. Sambles, Phys. Rev. Lett. **88**, 088301 (2002).
[42] P. D. Brimicombe, S. J. Elston, and E. P. Raynes, Liq. Cryst. **34**, 641 (2007).
[43] M. S. Kwon, J. W. Choi, and S.-W. Lee, IEEE Trans. Consum. Electron. **54**, 1459 (2008).
[44] M. Grinfeld, M. Langer, and N. J. Mottram, Liq. Cryst. **38**, 981 (2011).
[45] P. G. de Gennes and J. Prost, *The Physics of Liquid Crystals* (Clarendon, Oxford, 1995).
[46] G. Vertogen and W. H. de Jeu, *Thermotropic Liquid Crystals, Fundamentals* (Springer-Verlag, Berlin, 1998).
[47] T. Takahashi, S. Hashidate, H. Nishijou, M. Usui, M. Kimura, and T. Akahane, Jpn. J. Appl. Phys. **37**, 1865 (1998).
[48] F. Castles, S. C. Green, D. J. Gardiner, S. M. Morris, and H. J. Coles, AIP Adv. **2**, 022137 (2012).
[49] H. Pleiner and H. R. Brand, *Hydrodynamics and Electrohydrodynamics of Nematic Liquid Crystals, in Pattern Formation in Liquid Crystals*, edited by A. Buka and L. Kramer (Springer, New York, 1996), pp. 15–67.
[50] J. J. Arenzon, A. J. Bray, L. F. Cugliandolo, and A. Sicilia, Phys. Rev. Lett. **98**, 145701 (2007).
[51] The OpenFOAM package is accessible at http://www.openfoam.com/